This is a corrected version of the manuscript originally published presented at *International Conference on Modeling and Simulation of Microsystems, MSM 99*. The only correction is Eq 17.

A New Analytical Solution for Diaphragm Deflection and its Application to a Surface-Micromachined Pressure Sensor

William P. Eaton, Fernando Bitsie, James H. Smith, David W. Plummer
Sandia National Laboratories
P. O. Box 5800
Albuquerque, NM 87185-1081

ABSTRACT

An analytical solution for large deflections of a clamped circular diaphragm with built-in stress is presented. The solution is directly applicable to micromachined pressure sensors. The solution is compared to finite element analysis results and experimental data from a surface-micromachined pressure sensor.

Keywords: MEMS, microsystems, pressure sensor, diaphragm

INTRODUCTION

Several papers have recently been published regarding the deflection characteristics of micromachined diaphragms for application to pressure sensors and other acoustic devices [1-5]. For these devices, the applied load is assumed to be constant over the diaphragm surface. Optical and capacitive based devices measure diaphragm deflection directly, and deflected shape and amplitude is of importance. Piezoresistive devices, which are the focus of this work, measure deflection indirectly. Diaphragm stress is of importance in these devices.

Micromachined pressure sensors are currently a multibillion dollar industry. More than 16 million disposable blood pressure sensors and 25 million manifold absolute pressure sensors are produced annually [6]. Since pressure sensors are primarily diaphragm-based, it is important to have models for their stresses and strains, as well as diaphragm deflection.

In this work, we present an analytical solution for a clamped circular diaphragm with built-in stress and large deflections. In general, analytical and exact variational solutions for diaphragm behavior are desirable because of their ease of use and the insight they provide to the designer. Specific geometric effects can be ascertained from these solutions. However, these solutions are generally only applicable for small deflections. Numerical techniques, such as Finite Element Analysis, Boundary Element Analysis, and Finite Difference Analysis, can be more accurate in predicting deflection behavior, especially for large deflections. Unfortunately, these techniques generally require more effort to use and may not supply the same insight as analytical or exact variational solutions.

The use of plate theory is appropriate for the analysis of micromachined thin-film diaphragms. *Thin plate* or *small deflection* theory is often used, and is appropriate for deflections less than 1/5 of the diaphragm thickness [7]. *Large deflection* or *thick plate* theory is used for deflections up to three times the diaphragm thickness [7].

The work in this paper is unique, since it combines the effects of large deflections and built-in stresses, thereby unifying work reported by Suhir [8] and Voorthuyzen and Bergveld [1]. Both large deflections and built-in stresses are apt to be present in real-world micromachined devices, especially surface-micromachined devices. The analytical expression is compared to both finite element analysis results and experimental results from a circular, planar, surface-micromachined pressure sensor.

THEORY

Small Deflection/Membrane Theory

Solutions for small deflection theory and membrane theory are well known, but are repeated here for convenience. For small deflection, thin plate theory deflection is said to be dominated by the resistance of the diaphragm to bending. Deflection, w, of a clamped circular plate under a uniform applied pressure P is given by [7]

$$w(r) = \frac{Pa^4}{64D}\left[1-\left(\frac{r}{a}\right)^2\right]^2 , \tag{1}$$

where r, a, are the radial coordinate and diaphragm radius, respectively. D is the flexural rigidity, which is a measurement of stiffness, and is given by

$$D = \frac{Eh^3}{12(1-\nu^2)} , \tag{2}$$

where E, h, and ν are Young's modulus, plate thickness, and Poisson's ratio, respectively.

In contrast to small deflections theory, deflection in membrane theory is dominated by stresses in the plate [2]:

$$w(r) = \frac{Pa^2}{4\sigma_i h}\left[1-\left(\frac{r}{a}\right)^2\right] , \tag{3}$$

where σ_i is the intrinsic built-in stress of the plate.

Large Deflections with built in stress

The governing differential equations for the bending of a circular plate are [7, 8]

$$\nabla^4 w = \frac{P}{D} + \frac{h}{Dr}\frac{\partial\phi}{\partial r}\frac{\partial^2 w}{\partial r^2} \tag{4}$$

$$\nabla^4\phi = -\frac{E}{r}\frac{\partial w}{\partial r}\frac{\partial^2 w}{\partial r^2} \quad , \tag{5}$$

where ϕ is the Airy stress function and the biharmonic operator ∇^4 is given by (for azimuthal symmetry)

$$\nabla^4 = \left(\frac{\partial^2}{\partial r^2} + \frac{1}{r}\frac{\partial}{\partial r}\right)^2 \quad . \tag{6}$$

Most micromachined diaphragms are considered to have clamped boundary conditions, that is

$$w(r = edge) = 0, \quad \left.\frac{\partial w}{\partial r}\right|_{r=edge} = 0 \, . \tag{7}$$

An additional boundary condition is required to solve the problem. That is, that the amount of stretch, *u*, at the edge of the diaphragm is zero. This is further cast in terms of the circumferential strain through the center thickness of the diaphragm, ε_θ^0, and the built-in residual strain, ε_i i.e. [1]

$$u\big|_{r=a} = r\left(\varepsilon_\theta{}^0 - \varepsilon_i\right)\Big|_{r=a} = 0 \, . \tag{8}$$

This is further developed to become [1]

$$\begin{aligned} \varepsilon_\theta{}^0\Big|_{r=a} &= \frac{1}{E}\left(\sigma_\theta{}^0 - \nu\sigma_r{}^0\right)\Big|_{r=a} = \varepsilon_i \\ \Rightarrow \frac{\partial^2\bar{\phi}}{\partial r^2} - \frac{\nu}{r}\frac{\partial\bar{\phi}}{\partial r} &= \varepsilon_i E \quad . \end{aligned} \tag{9}$$

The deflection and Airy stress functions have the presumed solutions

$$w(r) = f\left(1 + C_1 r^2 + C_2 r^4\right) \tag{10}$$

$$\phi = f^2\left(B_1 r^2 + B_2 r^4 + B_3 r^6 + B_4 r^8\right), \tag{11}$$

where *f* is the maximum deflection of the plate. Applying the boundary conditions of Equation (7) to Equation (10) yields

$$w(r) = f\left[1 - \left(\frac{r}{a}\right)^2\right]^2 , \tag{12}$$

which has the same dependence on *r* as the small deflection case. This solution, when substituted into Equation (5), simplifies ϕ to

$$\phi(r) = f^2\left[B_1 r^2 - \frac{1}{4}\left(\frac{r}{a}\right)^4 + \frac{1}{9}\left(\frac{r}{a}\right)^6 - \frac{1}{48}\left(\frac{r}{a}\right)^8\right] . \tag{13}$$

If the boundary condition of Equation (9) is invoked, the solution for ϕ becomes

$$\phi(r) = \frac{f^2 E}{12}\left[\begin{array}{l}\left(\frac{5-3\nu}{1-\nu}\right)\left(\frac{r}{a}\right)^2 + \frac{\varepsilon_i}{2(1-\nu)}\left(\frac{r}{a}\right)^2 \\ -\frac{1}{4}\left(\frac{r}{a}\right)^4 + \frac{1}{9}\left(\frac{r}{a}\right)^6 \frac{1}{48}\left(\frac{r}{a}\right)^8\end{array}\right] . \tag{14}$$

The final step in the derivation is to solve for *f*. This is done by applying the Bubnov Galerkin method. But instead of using the energy functional as the coordinate, we minimize the governing differential equation of (4) and assume that *w(r)* is orthogonal with respect to all other coordinate functions, i.e.

$$\int_A w\left[D\nabla^4 w - \frac{h}{r}\left(\frac{\partial}{\partial r}\right)\left(\frac{\partial\phi}{\partial r}\frac{\partial w}{\partial r}\right) - P\right]dA = 0 \, . \tag{15}$$

Integrating and collecting terms gives

$$\frac{2Eh(1+\nu)(23-9\nu)}{63a^2(1-\nu^2)} f^3 + \frac{16Eh^3}{9a^2(1-\nu^2)} f - \frac{Pa^2}{3} = 0 \, . \tag{16}$$

This is a cubic equation with three roots. The real root of *f* is given by

$$\begin{aligned} f &= \sqrt[3]{-\frac{\beta}{2} + \gamma} + \sqrt[3]{-\frac{\beta}{2} - \gamma} \qquad \gamma = \sqrt{\frac{\alpha^3}{27} + \frac{\beta^2}{4}} \\ \alpha &= 14\frac{4h^2 + 3a^2\varepsilon_i(1+\nu)}{(1+\nu)(23-9\nu)} \qquad \beta = \frac{-7Pa^4h^2}{8D(1+\nu)(23-9\nu)} \quad . \end{aligned} \tag{17}$$

The function *w(r)* is plotted for both small and large deflection theory in Figure 1. The curves are nearly the same for small deflections and diverge for larger deflections, with thin plate theory overestimating the actual deflection. A marked reduction of deflection is predicted by the case of large deflections with stress.

The radial and circumferential stresses in the diaphragm, σ_r and σ_θ are given by [8]

$$\begin{aligned} \sigma_r &= -\frac{6D}{h^2}\left(\frac{\partial^2 w}{\partial r^2} - \frac{\nu}{r}\frac{\partial w}{\partial r}\right) + \frac{1}{r}\frac{\partial\phi}{\partial r} \\ \sigma_\theta &= -\frac{6D}{h^2}\left(\frac{1}{r}\frac{\partial w}{\partial r} - \nu\frac{\partial^2 w}{\partial r^2}\right) + \frac{1}{r}\frac{\partial^2\phi}{\partial r^2} \quad , \end{aligned} \tag{18}$$

and the strains can be calculated from the plane strain condition [8]:

$$\begin{aligned} \varepsilon_r &= \frac{1}{\mathrm{E}}\left(\sigma_r + \nu\sigma_\theta\right) \\ \varepsilon_\theta &= \frac{1}{\mathrm{E}}\left(\sigma_\theta + \nu\sigma_r\right). \end{aligned} \tag{19}$$

Output characteristics of a piezoresistive pressure

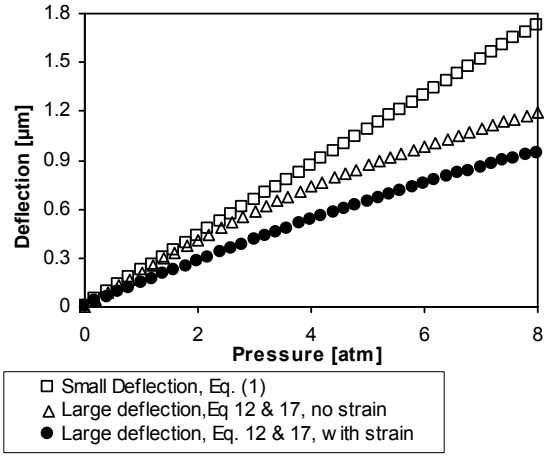

Figure 1. Deflection vs. Pressure for 100 µm diameter, Si_3N_4 diaphragm. E = 300 GPa, ν = 0.24, h = 1.2 µm, $\varepsilon_i = 5.5\cdot10^{-4}$.

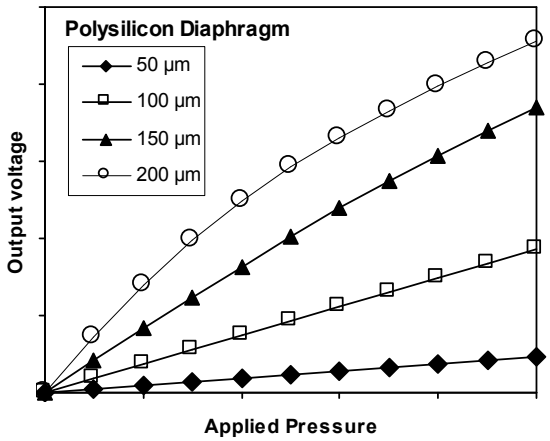

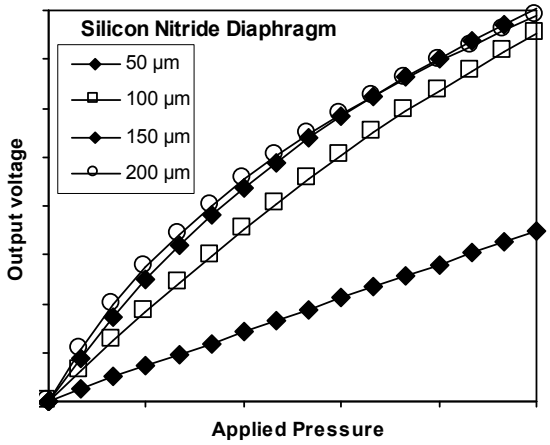

Figure 2. Prediction of piezoresistive pressure sensor characteristics for polysilicon (top) and silicon nitride (bottom) diaphragms. For polysilicon: E = 180 GPa, h = 2 µm, $\varepsilon_i = 5 \cdot 10^{-6}$. For nitride: E = 300 GPa, h = 1.4 µm, $\varepsilon_i = 5 \cdot 10^{-6}$.

similar to that shown in Figure 4 can be calculated using Equations 19 and examples are shown in Figure 2 for polysilicon and silicon nitride based diaphragms. The relatively high stress present in micromachined silicon nitride diaphragms has a profound effect on the output. Specifically, the 100, 150, and 200 µm diameter diaphragms all have similar sensitivity. This result is unexpected from small deflection theory.

FINITE ELEMENT ANALYSIS

Finite element analysis (FEA) is a valuable design tool for a diaphragm or sensor designer, since it generally gives more accurate results than analytical solutions. Perhaps even more important is the ability to model complex structures, which is difficult with analytical solutions. A circular diaphragm with fixed edges and a constant residual stress was modeled in Abaqus. The results are summarized in Figure 3 and are compared to the analytical solution for several diaphragm sizes. The results agree well, with the best agreement for the 100 µm diameter diaphragm.

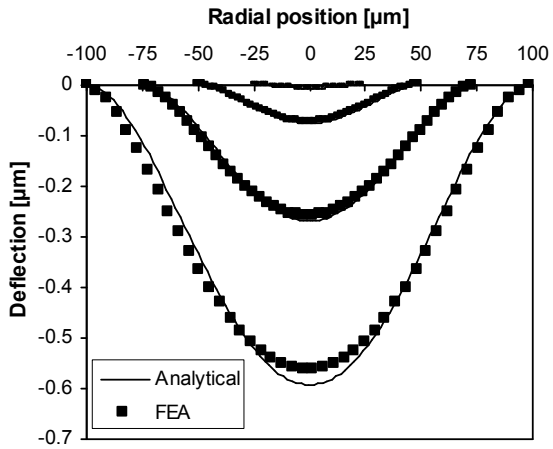

Figure 3. Comparison of FEA and analytical results for four silicon nitride diaphragm diameters: 50 µm, 100 µm, 150 µm, and 200 µm. P = 12 psi, E = 300 GPa, $\nu = 0.24$, h = 1.4 µm, $\varepsilon_i = 6.58 \cdot 10^{-4}$.

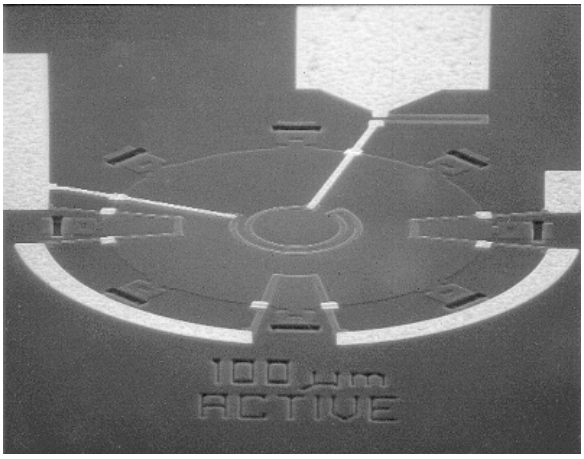

Figure 4. Scanning electron micrograph of surface micromachined pressure sensor diaphragm [9-12]. Diaphragm is 100 µm in diameter and has six radial and one circumferential piezoresistor(s).

EXPERIMENTAL DATA

A surface micromachined pressure sensor [9-12] is shown in Figure 4. It is a piezoresistive sensor and hence does not detect diaphragm deflection directly, but rather by changes in the diaphragm stress state. The output signal of the sensor is the output voltage of a Wheatstone bridge.

Deflection data for pressure sensors at a constant external pressure of 12 psi was extracted with a Wyko white light interferometer and is plotted in Figure 5, along with the analytical expression. The data agree fairly well, but discrepancies between the experimental data and the analytical expression of Equations 12 and 17 may be due to uncertainties in physical constants of the diaphragm (i.e. E and ν), residual stress, and diaphragm thickness. All of these parameters are difficult to measure with precision on micron scale structures.

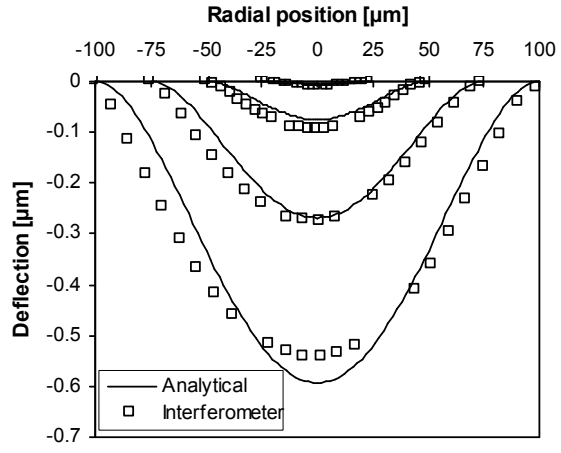

Figure 5. Comparison of FEA and analytical results for four silicon nitride diaphragm diameters: 50 µm, 100 µm, 150 µm, and 200 µm. P = 12 psi, E = 300 GPa, $\nu = 0.24$, h = 1.4 µm, $\varepsilon_i = 6.58 \cdot 10^{-4}$.

Output data from pressure sensors is shown in Figure 6. The results are qualitatively similar to the analytical model of Figure 2. The bending over of the 150 and 200 µm diameter nitride sensors is due to the diaphragms contacting the substrate. The 200 µm diameter curve is missing from the polysilicon diaphragm because of an incomplete release etch during device fabrication. As the analytical solution predicts, sensitivity clustering *does* occur in the silicon nitride diaphragm.

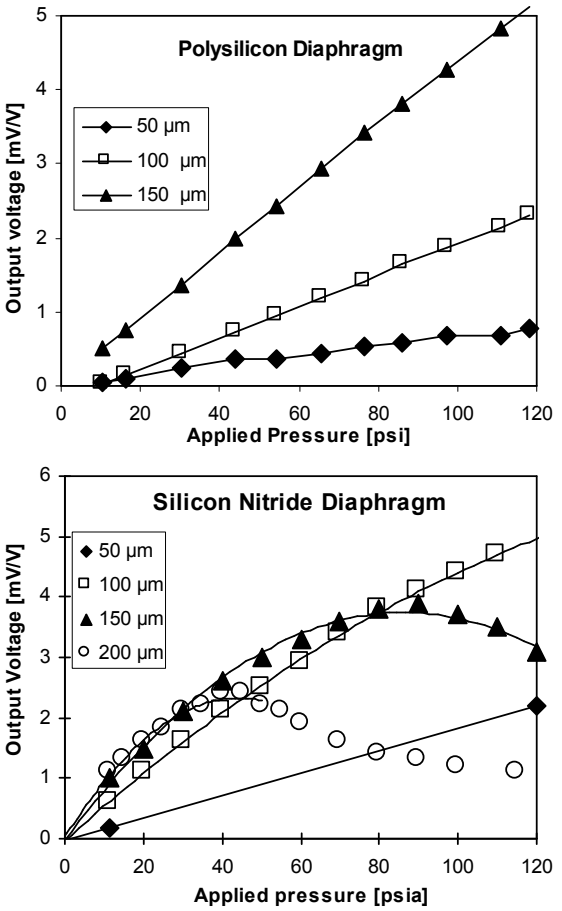

Figure 6. Experimental output voltage characteristics from devices similar to Figure 4 for polysilicon diaphragms (top) and silicon nitride diaphragms (bottom).

DISCUSSION & CONCLUSIONS

A new analytical solution for large deflections of a clamped, circular diaphragm with built-in strain has been presented. The solution agrees well with finite element analysis, but less well with interferometry from an actual surface-micromachined pressure sensor diaphragm. Imprecise data on Young's modulus and residual stress are likely contributors to this discrepancy. Nevertheless, the solution predicts the phenomenon of sensitivity clustering in nitride-based diaphragms. This solution is a powerful, easy to use tool for micromachinists.

ACKNOWLEDGMENTS

Sandia is a multiprogram laboratory operated by the Sandia Corporation, a Lockheed Martin Company, for the United States Department of Energy under contract DE-AC04-94-AL85000.

REFERENCES

[1] J. A. Voorthuyzen and P. Bergveld, *Sensors and Actuators*, **6**, pp. 201-213, (1984).
[2] R. Schellin, G. Hess, W. Kühnel, C. Thielemann, D. Trost, J. Wacker, and R. Steinmann, *Sensors and Actuators A*, **41-42**, pp. 287-292, (1994).
[3] D. Maier-Schneider, J. Maibach, and E. Obermeier, *Journal of Microelectromechanical Systems*, **4**(4), pp. 238-241, (1995).
[4] H. E. Elgamel, *Sensors and Actuators A*, **50**, pp. 17-22, (1995).
[5] R. Steinmann, H. Friemann, C. Prescher, and R. Schellin, *Sensors and Actuators A*, **48**, pp. 37-46, (1995).
[6] R. H. Grace, Guest editorial, *Sensors Magazine*, **16**(2), (1999).
[7] S. Timoshenko and S. Woinosky-Krieger, *Theory of Plates and Shells*, McGraw Hill Classic Textbook Reissue (1987).
[8] E. Suhir, *Structural Analysis in Microelectronic and Fiber-Optic Systems*, Volume I, Van Nostrand Reinhold (1991).
[9] W. P. Eaton and J. H. Smith, *Proceedings of Smart Structures and Materials 1995, Vol. 2448*, pp. 258-265 1995.
[10]W. P. Eaton and J. H. Smith, *Micro-machined Devices and Components II, Vol. 2882*, Austin, TX pp. 259-265 1996.
[11]W. P. Eaton and J. H. Smith, *Smart Materials and Structures*, **6**, pp. 530-539, (1997).
[12]W. P. Eaton, *Surface Micromachined Pressure Sensors*, Ph.D. Dissertation, University of New Mexico, 1997.